Wavelet based matrix compression in numerical micromagnetics

T. Schrefl, D. Süss and J. Fidler

Institute of Applied and Technical Physics, Vienna University of Technology,
Wiedner Hauptstr. 8-10/137, A-1040 Vienna, Austria, thomas.schrefl@tuwien.ac.at

ABSTRACT

Magnetic sensors and magneto-mechanic devices consist of spatially distinct ferromagnetic parts. Modeling their functional behavior requires to take into account the magnetostatic interactions between the magnetic elements. A hybrid finite element / boundary element method is combined with a wavelet matrix compression technique to simulate magnetization reversal of an array of magnetic nano-elements. This novel method reduces the storage requirements and the CPU time while keeping a reasonable accuracy. The boundary element matrix shows a sparsity of 80% to 90% with a corresponding relative error of the magnetic properties in the range of 2% to 5%. The calculated switching field of elongated NiFe nano-elements depends on magnetic state of neighboring elements. The spread in the switching field agrees with experimental data obtained from Lorentz electron microscopy.

Keywords: micromagnetics, finite elements, boundary elements, wavelets, matrix compression.

1 INTRODUCTION

The development of advanced magnetic materials such as magnetic sensors, recording heads, and magneto-mechanic devices requires a precise understanding of the magnetic behavior. These applications require a reproducible magnetic domain structure and a well-defined switching field of the individual magnetic elements [1]. As the size of the magnetic components approach the nanometer regime, detailed predictions of the magnetic properties becomes possible using micromagnetic simulations. Micromagnetism is a continuum theory for the treatment of magnetization processes in ferromagnetic materials. The micromagnetic equations describe the relation between the magnetic properties and the physical/chemical microstructure of the material. Micromagnetic simulation and magnetic imaging [2] are complementary tools to investigate domain formation and magnetization reversal. The comparison of simulations and experiments can provide useful hints for artificial structuring of the material, in order to tailor the magnetic properties according to their specific applications.

A key part in micromagnetic simulations is the calculation of the magnetic field which arises from the interaction of the magnetization with the element geometry. This so-called demagnetizing field is crucial for the formation of the magnetic domain structure in large elements and determines the external field required to reverse the magnetization of small elements. The magnetostatic interactions between distinct magnetic elements become important in magnetic multilayers or arrays of magnetic dots used for sensor applications, and magnetic storage [3,4].

The direct computation of the demagnetizing field from magnetic volume and surface charges [5] scales with n^2 in storage and computation time, where n denotes the number of grid points in a finite different or finite element discretization of the magnetic device. Fast adaptive algorithms have been applied in numerical micromagnetics using FFT or multipole expansion on regular computational grids [6], in order to speed up the calculations. Finite element based micromagnetic codes effectively treat the microstructure of the system, including the shape of the magnet and the irregular grain structure [8]. The FFT method cannot be applied on the corresponding unstructured mesh. Such as in finite element field calculation, micromagnetic finite element simulations introduce a magnetic scalar or magnetic vector potential to calculate the demagnetizing field [8]. Fredkin and Koehler [9] proposed a hybrid finite element (FE) / boundary element (BE) method to treat the open boundary problem associated with calculation of the magnetic scalar potential. This method is accurate and allows to calculate the magnetostatic interaction between distinct magnetic elements without any mesh between the magnetic particles. However, the conventional boundary element method requires to store a dense matrix.

This work introduces a novel method for micromagnetic simulations that combines a hybrid finite element (FE) / boundary element (BE) method with a wavelet matrix compression technique. A discrete wavelet transform using Daubechies wavelets is applied to transform the matrix obtained from the BE method into a sparse matrix. The computation of the dense matrix and its transformation has to be performed only once for a given geometry. The computational effort for field calculation reduces to a sparse-matrix vector product (BE part) and the solution of a sparse system of linear equations (FE part). The method was tested solving the µMAG standard problem #2 [10] and was applied to simulate the switching of an array of magnetic nano-elements. Section 2 of the paper presents the micromagnetic background. Section 3 describes the numerical model. Section 4 presents numerical results obtained for the µMAG standard problem and the magnetostatic interactions of elongated NiFe elements.

2 MICROMAGNETICS

2.1 Total magnetic Gibb's free energy

Micromagnetism starts from the total magnetic Gibb's free energy, E, of a ferromagnetic system, which is the sum of the exchange energy, the magneto-crystalline anisotropy energy, the magnetostatic energy, and the Zeeman energy [6]:

$$E = \int_{\Omega_m} \{ A \sum_{i=1}^{3} (\nabla \beta_i)^2 + f_k(\boldsymbol{J}) - \frac{1}{2} \boldsymbol{J} \cdot \boldsymbol{H}_d - \boldsymbol{J} \cdot \boldsymbol{H}_{ext} \} \, dV. \quad (1)$$

Here A denotes the ferromagnetic exchange constant, $\boldsymbol{J}$ is the magnetic polarization $\boldsymbol{J} = J_s(b_1, b_2, b_3) = \mu_0 \boldsymbol{M}$, and $\boldsymbol{M}$ is the magnetization. $\boldsymbol{H}_{ext}$ and $\boldsymbol{H}_d$ denote the external field and the demagnetizing field, respectively. $f_k(\boldsymbol{J})$ gives the magnetocrystalline anisotropy energy.

The subsequent minimization of (1) for different external fields, subject to the constraint $|\boldsymbol{J}| = J_s$, provides the hysteresis loop of a magnet [11]. The competitive effects of the micromagnetic energy contributions upon minimization determine the equilibrium distribution of the magnetization. The minimization of the ferromagnetic exchange energy aligns the magnetic moments parallel to each other, whereas the minimization of the magnetostatic energy favors the existence of magnetic domains. The magnetocrystalline anisotropy energy describes the interaction of the magnetization with the crystal lattice. Its minimization orients the magnetization parallel to certain crystallographic directions. The minimization of the Zeeman energy rotates the magnetization parallel to the external field.

2.2 Magnetostatic boundary problem

The demagnetizing field $\boldsymbol{H}_d$ follows from a magnetic scalar potential $\boldsymbol{H}_d = -\nabla U$. The magnetic scalar potential fulfills the Poisson's equation within the magnetic, Ω_m, and Laplace's equation outside the magnetic particle, Ω_e:

$$\nabla^2 U(\boldsymbol{r}) = \nabla \cdot \boldsymbol{M}(\boldsymbol{r}) \quad \text{for } \boldsymbol{r} \in \Omega_m, \quad (2)$$

$$\nabla^2 U(\boldsymbol{r}) = 0 \quad \text{for } \boldsymbol{r} \in \Omega_e, \quad (3)$$

At the surface of the magnet the boundary conditions

$$U^{in} = U^{out}, \quad (\nabla U^{in} - \nabla U^{out}) \cdot \boldsymbol{n} = \boldsymbol{M} \cdot \boldsymbol{n}, \quad (4)$$

hold, where $\boldsymbol{n}$ denotes the outward pointing normal unit vector. The magnetic scalar potential is regular at infinity.

3 NUMERICAL MODEL

The finite element method is applied to discretize the total magnetic Gibb's free energy. $\boldsymbol{M}(\boldsymbol{r})$ is approximated by piecewise linear function on a tetrahedral finite element mesh. Polar coordinates θ_i, φ_i for the magnetization at node i are introduced to satisfy the constraint $|\boldsymbol{J}| = J_s$ at the nodal points of the finite element mesh. A pre-conditioned, limited memory quasi-Newton conjugate gradient method [12] is applied to minimize the energy. Such as any algorithm for the solution of the micromagnetic problem, the conjugate gradient method may converge towards a saddle point [6,13]. To test for stability of a magnetic configuration, a small random perturbation was added and checked if it evolved back to its initial state.

Conjugate gradient based minimization techniques require only the energy and the gradient of the energy to search the local minima. The gradient of the energy may be expressed as

$$\frac{\partial E}{\partial \theta_i} = -V_i \boldsymbol{H}_{eff} \frac{\partial \boldsymbol{J}_i}{\partial \theta_i}, \quad \frac{\partial E}{\partial \varphi_i} = -V_i \boldsymbol{H}_{eff} \frac{\partial \boldsymbol{J}_i}{\partial \varphi_i}, \quad (5)$$

In (5) the effective field $\boldsymbol{H}_{eff}$ has been introduced. The effective field at the nodal point i of the finite element mesh can be approximated by

$$\boldsymbol{H}_{eff,i} = -\frac{\delta E}{\delta \boldsymbol{J}_i} \approx -\frac{1}{V_i} \frac{\partial E}{\partial \boldsymbol{J}_i}, \quad (6)$$

where V_i is the volume of a 'box' surrounding the nodal point i with

$$\sum_i V_i = \int_{\Omega_m} dV \quad \text{and} \quad V_i \cap V_j = 0 \text{ for } j \neq j. \quad (7)$$

Whereas the evaluation of the exchange field and the anisotropy field follows directly from (1), the calculation of the demagnetizing field $\boldsymbol{H}_d$ requires to solve the magnetostatic boundary value problem (2) to (4).

Following Fredkin and Koehler [10], we split the magnetic scalar potential into $U = U_1 + U_2$. The potential U_1 accounts for the divergence of magnetization within the particle and U_2 is required to meet the boundary conditions. The latter also carries the magnetostatic interactions between distinct magnetic particles. The potential U_1 is the solution of the Poisson equation

$$\nabla^2 U_1(\boldsymbol{r}) = \nabla \cdot \boldsymbol{M}(\boldsymbol{r}) \quad \text{for } \boldsymbol{r} \in \Omega_m \quad (8)$$

with the natural boundary condition

$$\nabla U_1 \cdot \boldsymbol{n} = \boldsymbol{M} \cdot \boldsymbol{n} \quad \text{for } \boldsymbol{r} \in \partial \Omega_m \quad (9)$$

and $U_1 = 0$ outside the magnetic particle. The potential U_2 satisfies the Laplace equation

$$\nabla^2 U_1(\boldsymbol{r}) = \nabla \cdot \boldsymbol{M}(\boldsymbol{r}) \quad \text{for } \boldsymbol{r} \in \Omega_m \cup \Omega_e \quad (10)$$

and shows a jump

$$U_2^{in} - U_2^{out} = U_1 \quad \text{for } \boldsymbol{r} \in \partial \Omega_m \quad (11)$$

at the boundary $\partial\Omega_m$. A standard finite element method is used to solve (8) and (9). Equations (10) and (11) define a double layer potential which is created by a dipole sheet at $\partial\Omega_m$ with magnitude U_1. At the surface $\partial\Omega_m$ the potential U_2 is given by the integral

$$U_2(\boldsymbol{r}) = \int_{\partial\Omega_m} U_1(\boldsymbol{r}')\nabla'\left(\frac{1}{|\boldsymbol{r}-\boldsymbol{r}'|}\right) d^2r' + \left(\frac{\Omega(\boldsymbol{r})}{4\pi} - 1\right) U_1(\boldsymbol{r}). \quad (12)$$

The solid angle $\Omega(\boldsymbol{r})$, subtended by $\partial\Omega_m$ at $\boldsymbol{r}$, equals 2π for a smooth surface point $\boldsymbol{r}$. After discretization of (12) using a boundary element method, the potential U_2 at the boundary follows from a matrix vector multiplication

$$\underline{U}_2 = \mathbf{B}\,\underline{U}_1 , \quad (13)$$

where $\mathbf{B}$ is a $m \times m$ matrix which relates the m boundary nodes to each other. Once U_2 at the boundary has been calculated, the values of U_2 within the particles follow from Laplace's equations with Dirichlet boundary conditions, which again can be a solved by a standard finite element technique.

A discrete wavelet transform is applied to transform the matrix $\mathbf{B}$ into a sparse matrix:

$$\mathbf{W}\,\underline{U}_2 = \mathbf{W}\,\mathbf{B}\,\mathbf{W}^{\boldsymbol{T}}\cdot(\mathbf{W}^{\boldsymbol{T}})^{-1}\underline{U}_1 , \quad (14)$$

where $\mathbf{W}$ is a matrix formed by Daubechies wavelets [14]. With the matrix $\mathbf{B}_w = \mathbf{W}\mathbf{B}\mathbf{W}^T$ in the new wavelet basis, the matrix vector product can be evaluated as follows

$$\underline{U}_{1,w} = (\mathbf{W}^{\boldsymbol{T}})^{-1}\underline{U}_1 , \quad (15)$$

$$\underline{U}_{2,w} = \mathbf{B}_w\,\underline{U}_{1,w} , \quad (16)$$

$$\underline{U}_2 = \mathbf{W}^T\,\underline{U}_{2,w} . \quad (17)$$

The matrix $\mathbf{B}_w$ has to be computed only once for a given geometry. All elements of $\mathbf{B}_w$ smaller in magnitude than δ times the largest element were set to zero. Thus $\mathbf{B}_w$ becomes sparse and (14) which significantly reduces the storage requirements and computation time for the calculation of $\underline{U}_2$. A reasonable accuracy can be obtained with a sparsity

$$S_\delta = \frac{m - m_\delta}{m} \times 100 \quad (16)$$

in range from 80% to 90%, where m_δ is the total number of elements after thresholding. The discrete wavelet transform provided in [14] and a sparse matrix toolkit were used for the calculations.

4 APPLICATIONS

The new algorithm was tested solving the micromagnetic standard problem #2 [10]. The demagnetization curve of a NiFe bar with the extension of 50 nm x 250 nm x 5 nm is calculated under an oblique applied field. Figure 1 depicts the particle configuration. The following material parameters where used for the calculations: zero magnetocrystalline anisotropy, the magnetic polarization J_s = 1 T, and the exchange constant A = 10^{-11} J/m.

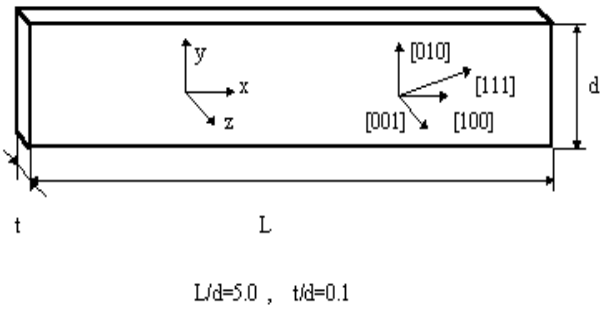

Figure 1:Geometry of the µMag Standard Problem #2. The external field is applied parallel to the [111] direction.

The original BE matrix consists of 1.3×10^6 elements. Figure 2 shows the sparsity pattern of the transformed matrix after thresholding using a threshold parameter $\delta = 10^{-3}$. The transformed matrix contains only 1.1×10^5 nonzero elements, giving a percent sparsity S_δ = 91.

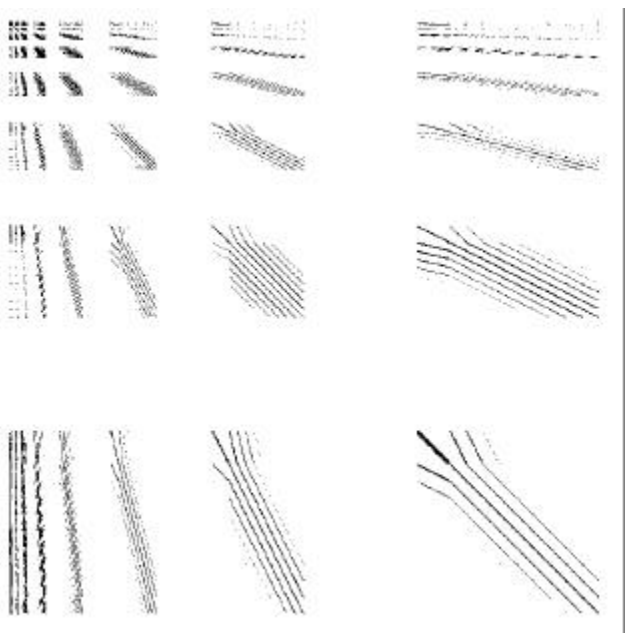

Figure 2: Sparsity pattern of the BE matrix after wavelet transformation using a threshold parameter $\delta = 10^{-3}$.

Figure 3 gives the percent sparsity S_δ, and the relative errors in the remanent magnetization and the switching field as a function of the threshold parameter δ. The relative error in the magnetic properties increases from 2% to 12% as the

threshold parameter is increased from 10^{-4} to $2x10^{-3}$. The corresponding values of the percent sparsity are 75% and 94%, respectively. Figure 4 compares calculated demagnetization curves for different threshold parameters with the solution obtained form the conventional FE / BE algorithm.

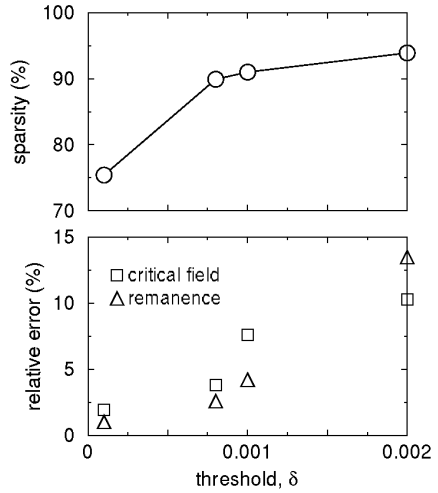

Figure 3: Percent sparsity and relative errors of the switching field (□) and the remanent magnetization (△) for the µMag 2 problem.

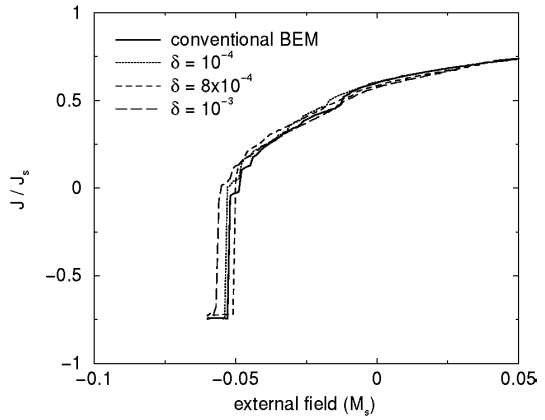

Figure 4: Calculated demagnetization curves using conventional FE/BE method and wavelet matrix compression.

Finally the method was used to simulate magnetization reversal in an array of NiFe nanoelements. Figure 5 gives the finite element model of three interacting nanoelements. Kirk and co-workers investigated NiFe elements of the very same aspect ratio and the same center to center spacing using Lorentz microscopy. The calculated switching field of an individual element depends on the magnetic state its neighbors. The magnetostatic interaction field is opposite to the magnetization. A pair of unswitched neighbors favors magnetization reversal in the center element, whereas two switched neighbors stabilize the center element. The calculated spread in the switching field was found to depend strongly on the threshold parameter δ. A value of $\delta < 10^{-5}$ was required to reach the interaction field of about 7 kA/m obtained with the conventional FE/BE method. The corresponding sparsity is $S_\delta < 80\%$. The dependence of the switching field on the number of switched neighbors is in qualitative agreement with the experiments.

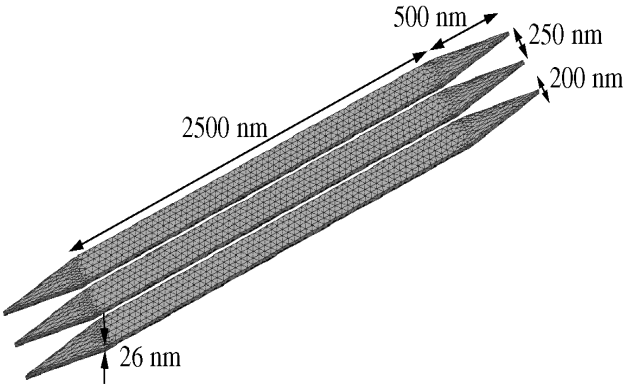

Figure 5: Finite element mesh of three magnetostatically interacting magnetic nanoelements.

ACKNOWLEDGMENT

This work was supported by the Austrian Science Fund (Y123-PHY).

REFERENCES

[1] K. J. Kirk, J. N. Chapman and C. D. W. Wilkinson, Appl. Phys. Lett. 71, 539, 1997.

[2] E. D. Dahlberg and J. G. Zhu, Physics Today 48, 34, 1995.

[3] S. Y. Chou, Proceedings of the IEEE 85, 652, 1997.

[4] R. P. Cowburn, A. O. Adeyeye and M. E. Welland, New-Journal-of-Physics 1, 1998-1999.

[5] A. Aharoni, "Introduction to the Theory of Ferromagnetism", Oxford University Press, 1996.

[6] S. W. Yuan and H. N. Bertram, IEEE Trans. Magn. 28, 2031, 1992.

[8] T. Schrefl, J. Magn. Magn. Mater. 207, 45, 1999.

[9] D. R. Fredkin and T. R. Koehler, IEEE Trans. Magn. 26, 415, 1990.

[10] R. D. McMichael, M. J. Donahue, D. G. Porter and J. Eicke, J. Appl. Phys. 85, 5816, 1999.

[11] D. Kinderlehrer and L. Ma, IEEE Trans. Magn. 30, 4380, 1994.

[12] P. E. Gill, W. Murray and M. H. Wright, "Practical Optimization," London: Academic Press, 1993.

[13] A. J. Newell and R. T. Merrill, J. Appl. Phys. 84, 4394, 1998.

[14] W. H. Press, S. A. Teukolsky, W. T. Vetterling, B. P. Flannery, "Numerical recipes in Fortran 77: The art of scientific computing," Cambridge University Press, 1992.